Journal of Neuroscience Methods 399 (2023) 109981

Contents lists available at ScienceDirect

Journal of Neuroscience Methods

journal homepage: www.elsevier.com/locate/jneumeth

Short communication

Substantially improved gene transfer to interneurons with second-generation glutamate receptor-targeted DART-AAV vectors

D.M. Günther [a], R. Kovacs [b], F. Wildner [b], A. Salivara [b], F.B. Thalheimer [c], P. Fries [a,d], J.R.P. Geiger [b], C.J. Buchholz [c,*]

[a] Ernst Strüngmann Institute (ESI) for Neuroscience in Cooperation with Max Planck Society, 60528 Frankfurt, Germany
[b] Institut für Neurophysiologie, Charité - Universitätsmedizin Berlin, Corporate Member of Freie Universität Berlin, Humboldt-Universität zu Berlin, Berlin Institute of Health, 10117 Berlin, Germany
[c] Molecular Biotechnology and Gene Therapy, Paul-Ehrlich-Institut, 63225 Langen, Germany
[d] Donders Institute for Brain, Cognition and Behaviour, Radboud University Nijmegen, 6525 EN Nijmegen, the Netherlands

ARTICLE INFO

Keywords:
DART-AAV
Capsid engineering
Hippocampal slice culture
Parvalbumin
Inhibitory neuron

ABSTRACT

Background: Adeno-associated viral vectors (AAVs) are a widely used gene transfer platform in neuroscience. Although naturally AAV serotypes can have preferences for certain tissues, selectivity for particular cell types in the CNS does not exist. Towards interneuron targeting, capsid engineering of AAV2 including display of the designed ankyrin repeat protein (DARPin) 2K19 specific for the glutamate receptor subunit 4 (GluA4) at the N-terminus of the VP2 capsid protein has been established. The resulting AAV-VP2N is highly specific for interneurons, but exhibits rather moderate transduction efficiencies.

Methods: Two alternative insertion sites for 2K19 in the GH2/GH3 loop of capsid proteins VP1 (AAV-VP1L) or VP2 (AAV-VP2L) were exploited to yield second generation GluA4-AAVs. Having packaged reporter genes under ubiquitous promoters, the vectors were characterized for biochemical properties as well as gene delivery into cell lines and rat hippocampal slice cultures. Electrophysiological recordings monitored the functional properties of transduced cells.

Results: Compared to AAV-VP2N, the second-generation vectors, especially AAV-VP1L, achieved about 2-fold higher genomic titers as well as a substantially improved GluA4 binding. Improvements in gene transfer activities were 18-fold on GluA4-overexpressing A549 cells and five-fold on rat hippocampal organotypic slice cultures reaching approximately 60 % of all parvalbumin positive interneurons upon a single administration. The spiking behaviour of transduced cells was unaltered and characteristic for a heterogeneous group of interneurons.

Conclusion: The substantially improved gene transfer activity of the second generation GluA4-targeted AAV combined with low toxicity makes this vector an attractive tool for interneuron-directed gene transfer with unrestricted promotor and transgene choice.

1. Introduction

Adeno-associated viral vectors (AAVs) are widely used as platform for gene transfer in neuroscience research (Nectow and Nestler, 2020). Applications include genetic delivery of reporters, sensors and effectors e.g. for gene function studies and disease models. Due to the ability to transduce dividing and especially non-dividing cells for long-term transgene expression in various animal models as well as in humans, AAVs have become the prime vector tool for the central nervous system (CNS) (Zhu et al., 2021).

AAVs are small, non-enveloped particles carrying a single-stranded DNA genome. The capsid is composed of VP1, VP2 and VP3 proteins at a ratio of 5:5:50. VP1 carries a phospholipase A2 (PLA2) domain necessary for endosomal escape, making it essential for gene transfer (Girod et al., 2002). Although naturally occurring serotypes can have preferences for certain tissues, selectivity for particular cell types including those of the CNS has not been observed. For cell entry, most AAV serotypes use modifications on surface proteins for cell attachment

* Corresponding author.
E-mail address: Christian.buchholz@pei.de (C.J. Buchholz).

https://doi.org/10.1016/j.jneumeth.2023.109981
Received 28 July 2023; Received in revised form 10 September 2023; Accepted 29 September 2023
Available online 30 September 2023

followed by contacting the AAV receptor (AAVR) for membrane penetration and intracellular transport (Pillay et al., 2016).

To tackle cell-type specific delivery, capsid engineering is performed using either library-based or rational based engineering. For evolutionary approaches, large numbers of capsid variants have been successfully screened, but missing information about the receptor(s) used by the identified capsids can prevent their use in other species (Buning and Srivastava, 2019; Hordeaux et al., 2018). In the rational approach, a high-affinity binder for the target receptor expressed on the cell type of choice is displayed on the AAV2 capsid. These can be designed ankyrin repeat proteins (DARPins) or nanobodies. Simultaneously, natural attachment to heparan-sulfate proteoglycan (HSPG) is ablated by mutating R585A and R588A (Buchholz et al., 2015).

With this approach a series of target receptors mainly relevant in cancer and immunotherapy have been addressed (Munch et al., 2015). More recently, the concept was adopted to target interneurons. DARPin 2K19 specific for the glutamate receptor subunit 4 (GluA4), which is highly expressed on parvalbumin positive (PV+) interneurons (Fuchs et al., 2007; Geiger et al., 1995), was fused to the VP2 N-terminus of AAV2 (Hartmann et al., 2018). The corresponding GluA4-AAV requires GluA4 as well as AAVR for successful gene delivery. While GluA4-AAV mediated specific interneuron targeting after intracranial injection into the mouse brain, its gene delivery activity remained moderate likely due to insufficient surface display of 2K19 and presence of VP2-deficient particles in vector stocks. Based on an alternative capsid insertion site, the GH2/3 loop in VP1, T-cell specific nanobodies and DARPins were recently successfully displayed on AAV2 (Eichhoff et al., 2019; Michels et al., 2021).

Here we exploited the GH2/3 loop for designing second generation GluA4-AAVs. Comparing the loop insertion into VP2 and VP1, especially AAV-VP1L assembled unimpaired, displayed 2K19 readily accessible at its surface, contained higher genome copies and was equally active in gene transfer as the first-generation vector. On rat hippocampal slice cultures, gene delivery into interneurons was highly efficient, with electrophysiological recordings confirming delivery into fast spiking interneurons.

2. Methods

2.1. Plasmids

To insert the coding sequence of 2K19 into the GH2/3 loop of AAV2 VP2, three fragments were generated via PCR on pGluA4.2K19-VP2 (Hartmann et al., 2019) as template (Table S1) using primers 2408/2409 (1), 2410/2411 (2), and 2412/2413 (3). Fragments were cleaved with *Nhe*I/*Pvu*I (1); *Pvu*I/*Spe*I (2); *Spe*I/*Sac*I (3) and were ligated into *Nhe*I/*Sac*I cleaved pGluA4.2K19-VP2 to produce pGluA4.2K19-VP2L. For inserting 2K19 into the GH2/3 loop of VP1, the *Bsi*WI/*Xcm*I fragment of pGluA4.2K19-VP2L was inserted into pRC_RR_VP1_r1c3 (Addgene: 65724) resulting in pGluA4.2K19-VP1L. To generate a packaging plasmid expressing only VP2 and VP3 for combination with pGluA4.2K19-VP1L, we ablated the VP1 start codon and reset that of VP2 in pRC-VP2-KO. Part of the coding sequence spanning the VP1 and the VP2 start codons was amplified on pRC-VP2-KO as template (primer 2529/2530 (1); 2531/2532 (2),) merged by overlap extension PCR (primers 2529/2532) and cloned into *Bsi*WI/*Swa*I restricted pRC-VP2-KO to generate pRC-VP1-KO (Table S1). Transfer vector plasmids pscAAV-CMV-eYFP was derived from (Hartmann et al., 2019) and pAAV-CAG-GFP from Vector Core Charité Berlin.

2.2. Western blot

Iodixanol gradient purified AAV samples were incubated in urea buffer (200 mM Tris/HCl [pH 8.0], 5 % SDS, 8 M urea, 0.1 mM EDTA, 2.5 % DTT, 0.03 % bromophenol blue) at 95 °C for 15 min and loaded onto a gradient SDS-PAGE (4–15 %). Separated proteins were blotted onto nitrocellulose membranes (Amersham, Amersham, UK, 10600004) which were incubated with the B1 antibody (1:50, Progen, Heidelberg, Germany, 61084) over night at 4 °C followed by rabbit anti-mouse immunoglobulin-HRP conjugate (1:2000, Agilent, P0260) for 2 h at room temperature (RT). Chemiluminescent peroxidase substrate (Sigma-Aldrich, CPS160–1KT) was applied and signal detected on the chemiluminescence reader MicroChemi (DNR Bio-Imaging Systems, Neve Yamin, Israel).

2.3. Transmission electron microscopy (TEM)

Formvar-carbon–coated 200-mesh nickel grids (Plano, G202N) were placed onto a 20 μL drop of AAV stock for 10 min at RT. Particles were contrasted by incubation in 1 % phosphotungstic acid at RT for 20 s. Samples were examined with Zeiss 109 TEM.

2.4. Enzyme-linked immunosorbent assay (ELISA)

For detection of the myc-tag on the DARPin, equal genome copies of AAV stocks were coated onto a 96-well Maxisorb plate and blocked (0.5 % BSA in PBS). Wells were incubated with anti-myc antibody (1:1000, Abcam, Ab18185) for 60 min at RT followed by an HRP-conjugated anti-mouse antibody (1:1000, Agilent, P0260). Signal was visualized by adding chemiluminescent peroxidase substrate (KPL (52−00−02)) and incubating at RT for 5 min before stopping the reaction.

Binding of GluA4 to AAVs was determined by sandwich ELISA using A20 coated plates (Progen, PRATV) for particle binding according to manufacturer's instructions. Biotinylated, ratGluA4 protein (self-produced (Hartmann et al., 2018)) was added further following the manufacturer's instructions for detection using the Infinite® Microplate reader M1000 (Tecan).

2.5. Production of AAV

AAV particles were generated using the adenovirus-helper-free AAV-packaging strategy and then purified and stored as described before (Hartmann et al., 2019). Plasmid amounts for the different vectors are provided in Table S2, genome copies were determined via ITR-specific qPCR using primers 15, 16, and probe 17 (Table S1) (Michels et al., 2021).

2.6. Transduction of cells and tissues

For transduction, 8E3 cells of the respective cell line were seeded per well into a 96-well plate. The next day, a dilution series of vector stocks starting at 1.3E6 gc/cell in 1:6 dilution steps were added. 72 h later flow cytometry was performed to determine the number of transduced viable cells (Fixable Viability Dye eFlour780 (Thermo Fisher Scientific, 65–0865–14)) using a MACSQuant Analyzer 10 (Miltenyi Biotec). Data analysis was performed using FCS Express 6 (De Novo Software).

2.7. Rat hippocampal slice cultures

Animal care and slice culture preparation was approved by the State Office of Health and Social Affairs Berlin (license number T-CH 003/2020). Each preparation (according to (Stoppini et al., 1991)) included two animals, and slices were not differentiated between individuals. Briefly, Wistar rats of either sex were sacrificed at postnatal day 6–7, the hippocampi extracted and rinsed in ice-cold, gassed minimal essential medium (MEM). Isolated hippocampi were aligned and cut into 400 μm slices perpendicular to the dorsoventral axis with a McIllvain Tissue Chopper. Slices were seeded on polytetrafluoroethylene (PTFE) membranes (Millicell-CM, Millipore) and maintained in six-well plates filled with 1 mL culture medium in a humidified CO_2 incubator (5 % CO_2). Medium was changed the day after preparation and thereafter three times a week. As the electrophysiological properties of the fast spiking

interneurons maturate *in vitro* into their adult form (Hasam-Henderson et al., 2018), recordings were obtained from day *in vitro* (DIV) 7–15. As control we used interneuron recordings from age-matched sister cultures. We labelled non-accommodating interneurons in control cultures with carboxymethyl 2′,7′-dichlorodihydrofluorescein (CM-H_2DCF) (Gotti et al., 2021). (20 μM, solved in DMSO, final dilution 0.1 %) for at least 20 min in the incubator prior to recording. Slice cultures were exposed to AAVs on DIV 2 by applying 5 μL of vector stock on top of each culture (2–3 cultures per membrane, final dilution 10–15 μL/mL) and incubated for 72 h. Cultures were imaged daily until DIV 15 (NIKON A1rm, AMBIO.charite.de).

2.8. Electrophysiology

Electrophysiological recordings were performed as described in (Gotti et al., 2021). Data were filtered at 3 kHz, digitized at 10 kHz (Digidata 1440 A, Axon CNS, Molecular Devices, Sunnyvale, CA, USA or EPC9, HEKA) and recorded by using the software Clampex 10 (Molecular Devices) or PatchMaster (HEKA, Heidelberg, Germany). Zero net current membrane potential (E_m), membrane capacity (C_m), membrane resistance (R_m) and access resistance (R_a), were determined automatically immediately after breakthrough. Recordings with unreliable Em (holding current $>$ 100 pA to maintain Em in CC) and/or Rm $<$ 3 *Ra were not included in the evaluation. In current clamp mode (CC), bridge balance was automatically compensated before recording 1 s long hyperpolarizing and depolarizing steps of 25 mV to evoke action potential (AP)-trains. Analysis was conducted using Clampfit (Molecular Devices), FitMaster (HEKA) and custom-made scripts for Mathworks, Matlab (9.9) software. For adaptation index, individual interspike intervals (ISIs) were calculated and adaptation index was defined as (Last 5 ISIs / First 5 ISIs). AP threshold was defined as the deflection point at the initial rise with at least $\frac{\partial}{\partial t}E(t) = 20mV/s$. AP halfwidth was calculated at half amplitude between spike maximum and minimal potential at fast afterhyperpolarization.

2.9. Immunohistochemistry

Slice cultures were fixed with 4 % paraformaldehyde/4 % sucrose in PBS 0.1 M over night at 4 °C and stored in 30 % sucrose/PBS. For immunolabelling, slices were carefully detached from the PTFE membranes and processed free-floating. Incubation with a mouse derived anti-parvalbumin antibody (1:1000; Millipore) in 0.1 % Triton X-100/PBS for 3 nights was followed by incubation for 24 h either with a goat anti-mouse Cy3 or Alexa 405 secondary antibody (1:100; Millipore) in case additional biocytin filled interneurons were labelled with avidin-conjugated Cy3 (1:1000, Invitrogen). Slices were mounted on adhesion slides (Superfrost Plus, Fisher Scientific) and coverslipped with Fluoromount-G (SouthernBiotech).

2.10. Imaging

Slice cultures were monitored either with a spinning disk confocal microscope (Andor Revolution, BFIOptilas GmbH, Gröbenzell, Germany) or with an epifluorescent microscope equipped with a CCD camera (XM10, Olympus, Japan). A z-stack of confocal images were taken prior to recording of a chosen cell, allowing for subsequent identification after biocytin labelling. Whole slice imaging of GFP fluorescence in the living tissue as well as the immunofluorescence reconstruction were made with a NIKON A1R MP multiphoton microscope (25x N.A. 1.1 objective, Nikon, Amsterdam, The Netherlands) at the AMBIO Life Cell Imaging Core Facility (AMBIO.charite.de). Reconstructions of the hippocampal slices were made from tile scans (5 × 4 tiles, 10 % overlap) covering the entire DG and cornu ammonis. Image analysis was performed using Cell Profiler (CellProfiler 4.2.4) for segmentation.

2.11. Statistical analysis

All statistical analyses were performed using GraphPad Prism version 9.5.0. Statistical significance was determined on population means using the one-way ANOVA (Tukey's multiple comparison test, alpha 0.05) for comparing the efficiency, and 2way ANOVA (Tukey's multiple comparison test, alpha= 0.05) for comparing the areas within the VP2N- and VP1L-groups.

3. Results

The GluA4-specific DARPin 2K19 was inserted into the GH2/3 loop of the VP1 or VP2 capsid protein of AAV2 on the genetic level (Fig. 1A). Thereby, seven amino acids of the GH2/3 loop (residues 453 – 459) of VP1 or VP2 were replaced by 154 amino acid residues covering 2K19, tags and linkers. To prevent the conformationally rigid DARPin from overstretching and destabilizing the GH2/3 loop as well as positioning it in an outward directed manner, we inserted a long flexible linker $(G_4S)_5$ at the N-terminus and a short G_4S linker at the C-terminus of 2K19. To ensure that the formed particles present the DARPin either on VP1 or VP2, the capsid proteins were expressed from two separate plasmids. For display on VP1, the expression of VP2 and VP3 was prevented by the deletion of the splice acceptor site downstream of the VP1 start codon resulting in plasmid pGluA4.2K19-VP1L. For display on VP2, the coding sequence for the VP1 N-terminus was deleted and that of 2K19 inserted into the GH2/3 loop of VP2 (pGluA4.2K19-VP2L). For vector particle generation, these plasmids were combined with plasmid pRC-VP1-KO, encoding VP2 and VP3 only, or, pRC-VP2-KO harbouring a mutated VP2 start codon for display on VP2. To prevent binding to the natural receptor of AAV2, HSPG binding was ablated by introducing R585A and R588A into all plasmids (Suppl. Fig. S1A).

Stocks of AAV-VP1L and AAV-VP2L reproducibly contained at least as many vector genomes as AAVmut and two-fold more than AAV-VP2N (Fig. 1B). Western blot analysis confirmed the incorporation of all three capsid proteins into the respective AAV stocks. Incorporation of the DARPin resulted in the expected shifts of about 20 kDa for VP1 and VP2 (Fig. 1C).

On A549 cells overexpressing GluA4 (A549-GluA4), all 2K19 displaying stocks showed selective transduction of A549-GluA4 cells (Fig. 1D). Remarkably, stocks harboring 2K19 in the GH2/3 loop were substantially more active in gene transfer than the first generation AAV-VP2N vector, reaching up to 34 % for AAV-VP2L and even 51 % for AAV-VP1L (Fig. 1E). This corresponded to an increase in gene transfer activities of about 8-fold for AAV-VP2L and 18-fold for AAV-VP1L (Fig. 1F). Electron microscopy of AAV-VP1L revealed the typical morphology of AAV particles with 87 % full particles (Fig. 1G, Suppl. Fig. 1C-D). While 2K19 was readily detectable in AAV-VP2N and AAV-VP1L via the myc-tag linked to 2K19 (Fig. 1H), only the second-generation vector showed a linear dose-response curve in binding soluble GluA4 (Fig. 1I), thus explaining the increased gene transfer activity by improved display and access of the DARPin. Like the first generation GluA4-AAV, AAV-VP1L also relied on the presence of AAVR for gene transfer into A549-GluA4 cells (Suppl. Fig. 1E-F).

To explore the transduction abilities of the vector stocks, hippocampal organotypic slice cultures were transduced and used for patch clamping as well as for histology. Microscopic evaluation revealed reporter gene expression throughout the whole slice culture for AAV-VP1L with substantially more transduced cells than for AAV-VP2N (Fig. 2A). Only very few transduced cells resembled non-neuronal astrocyte or oligodendrocyte morphology. The highest density of GFP-positive cells was observed in the hilus, as well as in CA3 *str. oriens* and *str. pyramidale*. Notably, none of these cells showed the typical pyramidal morphology of excitatory neurons (Fig. 2C). Around 60 % (95 % CI: 47.5–72.4 %) of PV+ cells expressed GFP with the AAV-VP1L vector, compared to only 18 % (95 % CI: 10.9–24.6 %) with the AAV-VP2N vector (Fig. 2B). The latter value corresponded well to the diluted VP1L stock (16 %, 95 % CI:

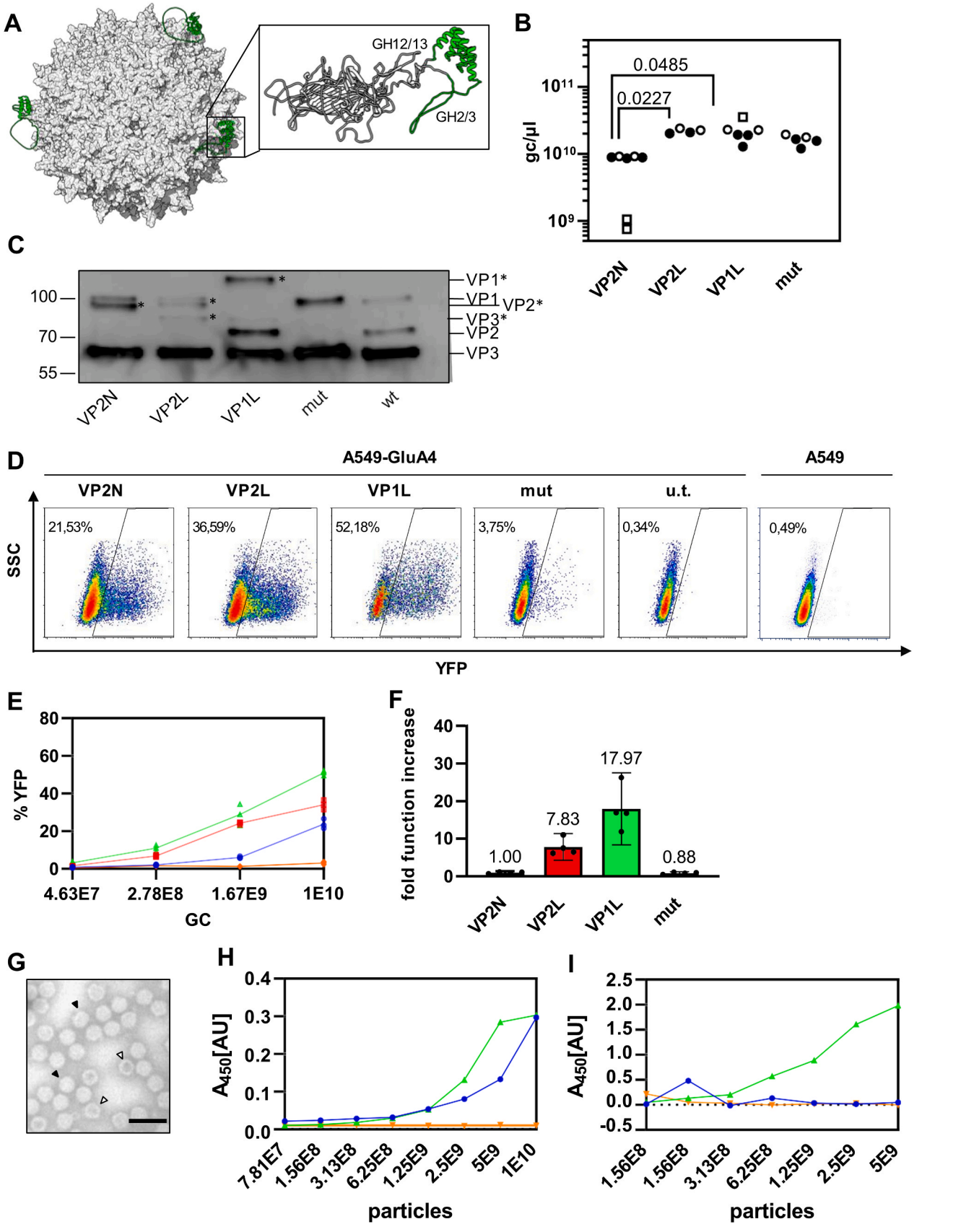

(caption on next page)

Fig. 1. Characterization of GluA4-targeted AAVs. Stocks of AAV-VP1L (VP1L, green), AAV-VP2L (VP2L, red), AAV-VP2N (VP2N, blue), AAVmut (mut, orange) and AAV2 (wt) were analysed. **A)** Structure of AAV-VP1L. Approximation of electron density surface of AAV2 capsid (grey) with 2K19 (green) inserted into the GH2/3 loop was calculated with Alpha Fold. **B)** Genome copies (gc) in vector stocks. Symbols represent technical replicates and different packaged genomes. Circles represent packaged CMV-YFP, squares CAG-GFP. Three qPCR runs of two stocks were used for statistical testing (one-way ANOVA) as indicated by the filled symbols. **C)** Western blot of the indicated vector types using the B1 antibody to visualize the capsid proteins VP1, VP2 and VP3 with (labelled by asterisk) or without 2K19. **D-F)** A549 cells stably expressing GluA4 or parental A549 were incubated with different doses of indicated AAVs or PBS (u.t.). Four days post transduction, eYFP expression was determined by flow cytometry. **D)** Representative flow cytometry plots showing sideward scatter versus eYFP signal of viable singlet cells transduced with 1E10 gc/well. **E)** Percentages of eYFP+ cells. Each symbol represents data from technical replicates (n = 3). **F)** Fold increase in transduction over AAV-VP2N. **G)** Electron microscopic image of AAV-VP1L. Black arrows indicate full particles, white arrows empty particles. Scale bar: 50 nm. **H)** Detection of displayed 2K19 via myc-tag ELISA. **I)** Detection of GluA4 binding to AAV particles via ELISA.

8.1–24.9 %) confirming a 5-fold increase in gene transfer activity of the second generation AAV-VP1L. This increase in activity did not compromise selectivity. Quantifications of four different hippocampal areas revealed equal selectivity of AAV-VP2N and AAV-VP1L for all areas except the dentate gyrus, where colocalization of PV and GFP was less pronounced (Suppl. Fig. 2B). However, all PV-negative, GFP-positive cells exhibited the typical morphology of interneurons.

For electrophysiology, we selected GFP expressing cells of neuronal morphology all over the hippocampus proper and the dentate gyrus. Their firing properties supported the characteristics of a heterogeneous population of interneurons (Fig. 2C). To clarify whether the AAV exposure affected the electrophysiological properties of the cells, we compared them with non-exposed age-matched sister cultures labelled with CM-H_2DCF. Comparison of basic electrophysiological properties revealed that vector-labelled and DCF-labelled interneuron populations were heterogeneous (Fig. 2D). Importantly, unaltered passive and active electrophysiological properties (Fig. 2D) showed that they were not affected by the vector particles. The slightly elevated resting membrane potential (E_m) of DCF labelled interneurons was likely due to the photoactivity of the fluorescent probe as this difference was present throughout all interneuron age groups (Suppl. Fig. 2C). Fast spiking interneurons are characterized by narrow action potentials, high frequency firing and a spike frequency adaptation index below 1.25 ((Petilla Interneuron Nomenclature et al., 2008), see S8). The median adaptation index in all three groups was below 1.25, AP half width below 0.6 ms, and the maximum firing frequency around 100 Hz or above. Interestingly, in all three groups, we found some cells with rather accommodating firing pattern as well as typical accelerating fast spiking interneurons with their action potential half width markedly differing between these types of interneurons (Fig. 2E). This heterogeneity was further supported by immunofluorescence labelling of the recorded cells against PV. Indeed, biocytin filled GFP+ interneurons showing accelerating firing pattern were PV+, whereas other GFP+ recorded cells with lower maximum firing frequencies were PV-negative (Fig. 2F).

4. Discussion

The second-generation GluA4-AAV vector described here is about five-fold more potent in gene delivery into hippocampal slice cultures than its first-generation counterpart, while having retained its dependency on GluA4 for cell entry. The improvement in gene delivery is due to a better presentation of the GluA4-specific DARPin on the particle surface, resulting in more efficient recognition of GluA4. It is likely that the alternative insertion site in VP1 is less prone to interfere with genome packaging and therefore better compatible with particle assembly than the VP2 N-terminus used in the first generation. Indeed, higher genomic titers were reproducibly found in second-generation stocks. Moreover, VP1 in contrast to VP2 is an essential part of the AAV capsid, while gene transfer competent VP2-deficient particles are commonly present in vector stocks (Hagen et al., 2014; Warrington et al., 2004). Accordingly, there is no need to get rid of DARPin-deficient particles by affinity chromatography for the second-generation vectors (Munch et al., 2015).

About 10 % of all neurons in the hippocampus are GABAergic interneurons, roughly 25 % of which are PV+ basket cells. On hippocampal slices from newborn rats, the second-generation GluA4-AAV showed a clear preference for interneurons. While PV-positive interneurons are known for high levels of GluA4 (Fuchs et al., 2007), also other types of interneurons do express GluA4 and were hit by the vector. Similarly, oligodendrocytes, which are easily distinguished from interneurons by their morphology, can be GluA4 positive (Kougioumtzidou et al., 2017) and were indeed transduced by GluA4-AAV. Apart from identification by morphology, the vector preference for interneurons was confirmed through the electrophysiological properties which overlapped with the DCF-accumulating cell population (Gotti et al., 2021).

While the hippocampal slice cultures show a strong indication for interneuron tropism, *in vivo* testing of the second generation GluA4-AAV will fully explore its tropism, since other brain areas might come with their own set of GluA4-positive cells. For example, the cerebellum harbours GluA4 expressing Bergman glia cells (Geiger et al., 1995). Moreover, tropism might differ in an adult brain as compared to the hippocampal slice cultures. Also, GluA4-positive oligodendrocyte precursors might not preserve their GluA4 expression during development to adult myelinating cells. Until *in vivo* experiments in the adult brain including areas like cortex, striatum and cerebellum have been performed, tropism for other cells than interneurons cannot be excluded.

Nevertheless, the second generation GluA4-AAV is applicable for a broad variety of neurophysiological research questions ranging from studies of gene functions to questions of neurodevelopment and neuronal networks. It is important to emphasize that its selectivity is mediated via the capsid at the level of cell entry, thus enabling unrestricted choice of genetic elements such as the promotor type. Use of a synapsin promotor for example, can detarget from non-neuronal cells. While going beyond the scope of the current manuscript, we anticipate that also *in vivo* gene delivery will be substantially improved by the second-generation vector. Accordingly, applications for therapeutic strategies addressing for example epilepsy or neuropsychiatric disorders including autism and Alzheimer's disease will benefit from targeted gene delivery into interneurons. The modular DART-AAV platform enables convenient exchange of the binder for the target receptor thus offering straight-forward targeting of other cell types of interest in the CNS.

CRediT authorship contribution statement

Dorothee Günther - experimental design, AAV generation and characterization, manuscript drafting. Frederic Thalheimer – experimental design, manuscript revision. Aikaterini Salivara – patch clamp recording of interneurons. Richard Kovacs - transduction and live imaging of the cultures, patch clamp recordings and imaging of the immunofluorescent preparations, data analysis, manuscript revision. Florian Wildner - patch clamp recording of GFP expressing or DCF accumulating interneurons, analysis of the electrophysiological data. Pascal Fries – study concept, manuscript revision. Jörg Geiger – study concept, data analysis, manuscript revision. Christian Buchholz – study concept, experimental design, manuscript drafting.

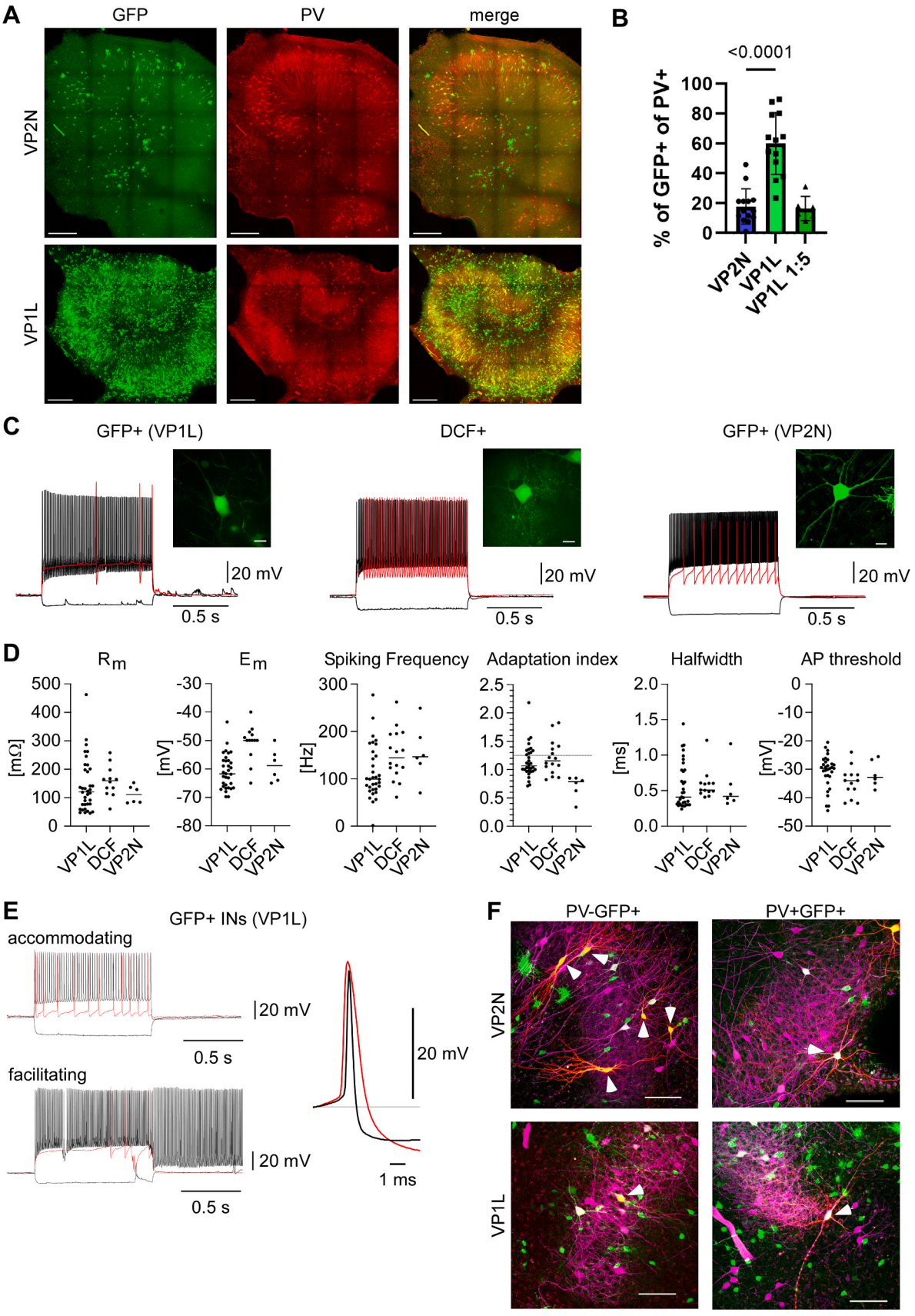

(caption on next page)

Fig. 2. Transduction of organotypic hippocampal slice cultures. Whole hippocampal slice cultures transduced with 9E8 - 1.7E11 gc/slice of AAV-VP2N (VP2N) or AAV-VP1L (VP1L) delivering the CAG-GFP construct. **A)** Microscopic overview of representative slices stained for PV. GFP fluorescence (GFP) and the overlay (merge) are shown. Scale bar: 300 μm **B)** Percentages of GFP+ cells among PV+ cells (AAV-VP2N: n = 14, AAV-VP1L: n = 13, AAV-VP1L 1:5: n = 6). P-value was calculated with one-way ANOVA. **C-F)** Whole cell patch clamp recordings from interneurons identified as GFP+ after transduction or DCF+ after labelling. **C)** Representative examples of the fluorescence images (upper panels) and characteristic membrane potential responses to current steps (hyperpolarizing, threshold, maximum frequency) are shown. Scale bar: 10 μm. **D)** Electrophysiological properties of GFP expressing and DCF labelled interneurons from age-matched sister cultures. From left to right, membrane resistance, membrane potential, maximum spike frequency upon a 1 s depolarisation step, adaptation index representing the ratio of the inter-spike interval of the last 5 to first 5 action potentials, action potential width at half maximum and the membrane potential threshold to elicit an action potential (see methods). **E)** GFP expressing interneurons presenting with accommodating (upper panel) and facilitating firing pattern (lower panel). **F)** Immunofluorescent labelling of PV in the recorded cells. PV negative (left) and PV positive (right) interneurons (arrows) after incubation with AAV-VP2N (upper panels) and AAV-VP1L. Scale bar: 100 μm.

Declaration of Competing Interest

P.F. has a patent on thin-film electrodes and is a member of the Advisory Board of CorTec GmbH (Freiburg, Germany). All other authors do not have any conflict of interests to declare.

Data availability

Data will be made available on request.

Acknowledgements

The authors like to acknowledge Andrea Wilke (Charité) for assistance with slice cultures, Charlotte Meierheinrich (Charité) for assistance with electrophysiological recording, Gundula Braun (PEI) for assistance with AAV productions, and Thorsten Trimbuch, Anke Schönherr and Nadine Albrecht-Koepke from the Viral Core Facility of the Charité– Universitätsmedizin Berlin (vcf.charite.de) for providing AAV-VP2N stocks. This work was supported by funding of the BMBF project COMMUTE (16GW0339) to C.J.B.

Appendix A. Supporting information

Supplementary data associated with this article can be found in the online version at doi:10.1016/j.jneumeth.2023.109981.

References

Buchholz, C.J., Friedel, T., Buning, H., 2015. Surface-engineered viral vectors for selective and cell type-specific gene delivery. Trends Biotechnol. 33, 777–790. ⟨https://www.ncbi.nlm.nih.gov/pubmed/26497425⟩.

Buning, H., Srivastava, A., 2019. Capsid modifications for targeting and improving the efficacy of AAV vectors. Mol. Ther. Methods Clin. Dev. 12, 248–265. ⟨https://www.ncbi.nlm.nih.gov/pubmed/30815511⟩.

Eichhoff, A.M., Borner, K., Albrecht, B., Schafer, W., Baum, N., Haag, F., Korbelin, J., Trepel, M., Braren, I., Grimm, D., Adriouch, S., Koch-Nolte, F., 2019. Nanobody-enhanced targeting of AAV gene therapy vectors. Mol. Ther. Methods Clin. Dev. 15, 211–220. ⟨https://www.ncbi.nlm.nih.gov/pubmed/31687421⟩.

Fuchs, E.C., Zivkovic, A.R., Cunningham, M.O., Middleton, S., Lebeau, F.E., Bannerman, D.M., Rozov, A., Whittington, M.A., Traub, R.D., Rawlins, J.N., Monyer, H., 2007. Recruitment of parvalbumin-positive interneurons determines hippocampal function and associated behavior. Neuron 53, 591–604. ⟨https://www.ncbi.nlm.nih.gov/pubmed/17296559⟩.

Geiger, J.R., Melcher, T., Koh, D.S., Sakmann, B., Seeburg, P.H., Jonas, P., Monyer, H., 1995. Relative abundance of subunit mRNAs determines gating and Ca2+ permeability of AMPA receptors in principal neurons and interneurons in rat CNS. Neuron 15, 193–204. ⟨https://www.ncbi.nlm.nih.gov/pubmed/7619522⟩.

Girod, A., Wobus, C.E., Zadori, Z., Ried, M., Leike, K., Tijssen, P., Kleinschmidt, J.A., Hallek, M., 2002. The VP1 capsid protein of adeno-associated virus type 2 is carrying a phospholipase A2 domain required for virus infectivity. J. Gen. Virol. 83, 973–978. ⟨https://www.ncbi.nlm.nih.gov/pubmed/11961250⟩.

Gotti, G.C., Kikhia, M., Wuntke, V., Hasam-Henderson, L.A., Wu, B., Geiger, J.R.P., Kovacs, R., 2021. In situ labeling of non-accommodating interneurons based on metabolic rates. Redox Biol. 38, 101798. ⟨https://www.ncbi.nlm.nih.gov/pubmed/33285412⟩.

Hagen, S., Baumann, T., Wagner, H.J., Morath, V., Kaufmann, B., Fischer, A., Bergmann, S., Schindler, P., Arndt, K.M., Muller, K.M., 2014. Modular adeno-associated virus (rAAV) vectors used for cellular virus-directed enzyme prodrug therapy. Sci. Rep. 4, 3759. ⟨https://www.ncbi.nlm.nih.gov/pubmed/24457557⟩.

Hartmann, J., Munch, R.C., Freiling, R.T., Schneider, I.C., Dreier, B., Samukange, W., Koch, J., Seeger, M.A., Pluckthun, A., Buchholz, C.J., 2018. A library-based screening strategy for the identification of DARPins as ligands for receptor-targeted AAV and lentiviral vectors. Mol. Ther. Methods Clin. Dev. 10, 128–143. ⟨https://www.ncbi.nlm.nih.gov/pubmed/30101151⟩.

Hartmann, J., Thalheimer, F.B., Hopfner, F., Kerzel, T., Khodosevich, K., Garcia-Gonzalez, D., Monyer, H., Diester, I., Buning, H., Carette, J.E., Fries, P., Buchholz, C. J., 2019. GluA4-targeted AAV vectors deliver genes selectively to interneurons while relying on the AAV receptor for entry. Mol. Ther. Methods Clin. Dev. 14, 252–260. ⟨https://www.ncbi.nlm.nih.gov/pubmed/31463334⟩.

Hasam-Henderson, L.A., Gotti, G.C., Mishto, M., Klisch, C., Gerevich, Z., Geiger, J.R.P., Kovacs, R., 2018. NMDA-receptor inhibition and oxidative stress during hippocampal maturation differentially alter parvalbumin expression and gamma-band activity. Sci. Rep. 8, 9545. ⟨https://www.ncbi.nlm.nih.gov/pubmed/29934499⟩.

Hordeaux, J., Wang, Q., Katz, N., Buza, E.L., Bell, P., Wilson, J.M., 2018. The neurotropic properties of AAV-PHP.B are limited to C57BL/6J mice. Mol. Ther. 26, 664–668. ⟨https://www.ncbi.nlm.nih.gov/pubmed/29428298⟩.

Kougioumtzidou, E., Shimizu, T., Hamilton, N.B., Tohyama, K., Sprengel, R., Monyer, H., Attwell, D., Richardson, W.D., 2017. Signalling through AMPA receptors on oligodendrocyte precursors promotes myelination by enhancing oligodendrocyte survival. Elife 6. ⟨https://www.ncbi.nlm.nih.gov/pubmed/28608780⟩.

Michels, A., Frank, A.M., Gunther, D.M., Mataei, M., Borner, K., Grimm, D., Hartmann, J., Buchholz, C.J., 2021. Lentiviral and adeno-associated vectors efficiently transduce mouse T lymphocytes when targeted to murine CD8. Mol. Ther. Methods Clin. Dev. 23, 334–347. ⟨https://www.ncbi.nlm.nih.gov/pubmed/34729380⟩.

Munch, R.C., Muth, A., Muik, A., Friedel, T., Schmatz, J., Dreier, B., Trkola, A., Pluckthun, A., Buning, H., Buchholz, C.J., 2015. Off-target-free gene delivery by affinity-purified receptor-targeted viral vectors. Nat. Commun. 6, 6246. ⟨https://www.ncbi.nlm.nih.gov/pubmed/25665714⟩.

Nectow, A.R., Nestler, E.J., 2020. Viral tools for neuroscience. Nat. Rev. Neurosci. 21, 669–681. ⟨https://www.ncbi.nlm.nih.gov/pubmed/33110222⟩.

Petilla Interneuron Nomenclature, G., Ascoli, G.A., Alonso-Nanclares, L., Anderson, S.A., Barrionuevo, G., Benavides-Piccione, R., Burkhalter, A., Buzsaki, G., Cauli, B., Defelipe, J., Fairen, A., Feldmeyer, D., Fishell, G., Fregnac, Y., Freund, T.F., Gardner, D., Gardner, E.P., Goldberg, J.H., Helmstaedter, M., Hestrin, S., Karube, F., Kisvarday, Z.F., Lambolez, B., Lewis, D.A., Marin, O., Markram, H., Munoz, A., Packer, A., Petersen, C.C., Rockland, K.S., Rossier, J., Rudy, B., Somogyi, P., Staiger, J.F., Tamas, G., Thomson, A.M., Toledo-Rodriguez, M., Wang, Y., West, D.C., Yuste, R., 2008. Petilla terminology: nomenclature of features of GABAergic interneurons of the cerebral cortex. Nat. Rev. Neurosci. 9, 557–568. ⟨https://www.ncbi.nlm.nih.gov/pubmed/18568015⟩.

Pillay, S., Meyer, N.L., Puschnik, A.S., Davulcu, O., Diep, J., Ishikawa, Y., Jae, L.T., Wosen, J.E., Nagamine, C.M., Chapman, M.S., Carette, J.E., 2016. An essential receptor for adeno-associated virus infection. Nature 530, 108–112. ⟨https://www.ncbi.nlm.nih.gov/pubmed/26814968⟩.

Stoppini, L., Buchs, P.A., Muller, D., 1991. A simple method for organotypic cultures of nervous tissue. J. Neurosci. Methods 37, 173–182. ⟨https://www.ncbi.nlm.nih.gov/pubmed/1715499⟩.

Warrington Jr., K.H., Gorbatyuk, O.S., Harrison, J.K., Opie, S.R., Zolotukhin, S., Muzyczka, N., 2004. Adeno-associated virus type 2 VP2 capsid protein is nonessential and can tolerate large peptide insertions at its N terminus. J. Virol. 78, 6595–6609. ⟨https://www.ncbi.nlm.nih.gov/pubmed/15163751⟩.

Zhu, D., Schieferecke, A.J., Lopez, P.A., Schaffer, D.V., 2021. Adeno-associated virus vector for central nervous system gene therapy. Trends Mol. Med. 27, 524–537. ⟨https://www.ncbi.nlm.nih.gov/pubmed/33895085⟩.